Instruments and Methods

Contact spectroscopy for determination of stratigraphy of snow optical grain size

Thomas H. PAINTER,[1] Noah P. MOLOTCH,[2] Maureen CASSIDY,[1] Mark FLANNER,[3] Konrad STEFFEN[4]

[1]National Snow and Ice Data Center/World Data Center for Glaciology, CIRES, University of Colorado, Boulder, Colorado 80309-0449, USA
E-mail: tpainter@nsidc.org
[2]Department of Civil and Environmental Engineering, University of California, Los Angeles, California 90095-1593, USA
[3]Department of Earth System Science, University of California, Irvine, California 92697-3100, USA
[4]Cooperative Institute for Research in Environmental Sciences, University of Colorado, Boulder, Colorado 80309-0216, USA

ABSTRACT. We present a technique for in situ measurement of the vertical and spatial stratigraphic distribution of snow optical grain size with a coupled contact illumination probe and field spectroradiometer. Accurate measurements of optical-equivalent grain size are critical for modeling radiative properties of snow such as spectral albedo and microwave emission. Measurements of the spectral reflectance of the snow-pit surface are made at 2 cm intervals in the vertical plane under constant illumination and view geometries. We invert the integral of the continuum normalization of the ice absorption feature with maximum at 1.03 µm wavelength for optical-equivalent grain size using the validated model of Nolin and Dozier (2000) that has accuracy of ±10–50 µm across the grain-size range 50–900 µm. Results are presented for an alpine site in southwest Colorado, USA, across the ablation season and for a Greenland ice-sheet site at the onset of snowmelt. These results suggest that traditional measurements of grain size using a hand lens are nearly accurate only for rounded grains ($R^2 = 0.41$, rmse $= 160$ µm); for polycrystals and faceted grains the hand-lens approach is very inaccurate ($R^2 = 0.03$ and 0.24, rmse $= 1206$ and 1010 µm, respectively). We demonstrate an order-of-magnitude improvement in modeling of shortwave spectral albedo and net shortwave flux with contact spectroscopy measurements of grain-size stratigraphy over those from a hand lens.

INTRODUCTION

The grain size of snow controls the optical properties of the snowpack (Warren, 1982) and indicates the advancement of metamorphism processes (Davis and others, 1993). The stratigraphy of snow grain size is critical for mechanical, thermodynamic and radiative properties of the snowpack (Colbeck, 1991; Pielmeier and Schneebeli, 2003). In situ observations of snow properties for hydrology and avalanche studies frequently include manual, hand-lens estimates of grain-size stratigraphy. The NASA/US National Weather Service (NWS) Cold Land Processes Experiments (CLPX) of 2002–03 in the western United States included a protocol for estimates of grain-size stratigraphy using a hand lens to provide modeling constraints for microwave radiative transfer models (D. Cline and others, http://nsidc.org/data/nsidc-0176.html). However, these manual measurements lack repeatability and do not infer the optical-equivalent grain size used for radiative transfer modeling. Quantitative and repeatable measurements of optical-equivalent grain size may be made through stereological techniques (Davis and others, 1987; Painter and Dozier, 2004), but these methods require extensive procurement of samples, delicate transport and many laboratory hours that necessarily span several days.

Accurate detection of snow grain size is particularly important for modeling applications where snow grain size is treated explicitly (e.g. *Crocus* (Brun and others, 1992),

SNOWPACK (Bartelt and Lehning, 2002) and SNTHERM (Jordan, 1991)). The logistical constraints and, in some cases, subjective nature of the aforementioned measurement techniques limit their applicability in supporting the development of physically based snow process models and therefore toward improving the land-surface, hydrologic and general circulation models that require representation of snowpack processes. In this regard, Jin and others (1999) found that complex models of snowpack processes do not improve upon more simplistic algorithms, largely due to inadequate representation of key snowpack states such as grain size.

Accurate measurements of snow grain size are also critical for the development of direct inversion techniques for estimating snow water equivalent (SWE) from microwave remote sensing (Armstrong and others, 1993; Kelly and others, 2003) and for estimating snow albedo and fractional snow-covered area (Li and others, 2001; Painter and others, 2003; Flanner and Zender, 2006). An improved representation of snow grain size within these direct retrieval algorithms is critical for solving the many-to-one relationships between SWE and brightness temperature that currently constrain retrieval accuracy (Foster and others, 2005). With regard to both improving representation of grain size as a model state and within direct inversion techniques, information about the variability in snow grain size and uncertainty in grain-size parameterizations has considerable utility within data-assimilation schemes aimed at bringing together measurements and models (Durand and Margulis, 2006).

Fig. 1. Contact probe with an unpainted slip-on spacer to facilitate view of configuration. The slip-on spacer that is implemented in the field has been coated with thick, flat black paint to occlude all radiation other than that from the probe illumination.

Here, we refer to grain size inferred from traditional hand-lens measurements as TGR (traditional grain radius) and optical-equivalent grain radius as OGR (optical grain radius). Given the subjective nature of TGR measurements, it is poorly defined and as such is not repeatable from observer to observer (personal communication from S. Colbeck, 2006). The OGR is well defined as the spherical grain radius required to give the same spectral or spectrally integrated albedo. OGR may also be represented by the specific surface area (surface area per unit volume ice) in the case of fluxes or albedo for snow (Dozier, 1989; Flanner and Zender, 2006; Matzl and Schneebeli, 2006) or clouds (Grenfell and Warren, 1999).

Matzl and Schneebeli (2006) presented a digital near-infrared (NIR) photographic technique for estimating snow specific surface area (SSA = 6/d where d is the sphere diameter). The photographic technique inverts based on a relationship between SSA, as determined with stereological analysis of select regions of the snow-pit face, and reflectance, and therefore requires a planar face for uniform illumination. Much higher spatial resolution imagery (~1 mm spatial resolution) of SSA can be derived from NIR photography than from the technique described in the present work (~2 cm). However, the photographic technique is not easily transferable because new stereological analyses are required for individual cameras, due to different spectral responses and the directional reflectance from the snow surface, and Spectralon panels used for reference depend strongly on changes in illumination conditions. As discussed below, the complementary coupling of the NIR photographic

technique (high spatial resolution) with the method described in the current paper (repeatable, transferable and accurate determination of SSA or OGR) should provide the highest possible accuracy and spatial resolution determination of snowpack SSA or OGR for field studies.

Here we present a technique for making rapid and accurate measurements of the stratigraphy of snow optical grain size. The technique couples an Analytical Spectral Devices (ASD) contact probe with an ASD FieldSpec FR field spectroradiometer and inverts the sampled ice absorption feature at 1.03 μm wavelength for OGR using the field and imaging validated, integral model of Nolin and Dozier (2000). While the technique does not provide the spatial resolution of the photographic technique, it has lower uncertainty due to the high signal-to-noise ratio and spectral resolution of the instrument and it is insensitive to illumination conditions.

We discuss the technique in terms of the spectro-radiometer and the contact probe, the spectroscopy model for retrieval of grain size and its previous validation, and results from alpine snow cover in southwest Colorado, USA, and from polar snow cover in West Greenland. We then present the differences between OGR and TGR for different grain shapes and show the order-of-magnitude greater accuracy in radiative transfer modeling with grain-size stratigraphy from contact spectroscopy over those from hand-lens retrievals.

METHODS

Instrumentation

The ASD FieldSpec FR spectroradiometer samples spectral radiance across the wavelength range 0.35–2.5 μm with spectral resolution of 0.003 μm at $\lambda \cong 0.7$ μm and 0.01 μm at $\lambda \cong 1.4$ and 2.1 μm. Its nominal noise equivalent changes in radiance (neΔL) are 1.4×10^{-9} W cm^{-2} nm^{-1} sr^{-1} at 0.7 μm, 2.4×10^{-9} W cm^{-2} nm^{-1} sr^{-1} at 1.4 μm and 8.8×10^{-9} W cm^{-2} nm^{-1} sr^{-1} at 2.1 μm. The contact probe (Fig. 1) has a stable light source integrated with the mount for the spectroradiometer optic cable (http://www.asdi.com). The contact probe light source is aligned at 23° to the probe body, and, with this fixed illumination zenith, the probe avoids problems of variable illumination from surface topography, may be implemented at any time of day and allows rapid acquisition. The light source is a halogen–krypton bulb with peak irradiance at wavelength $\lambda \sim 0.966$ μm and stability of 0.5% coefficient of variation and 0.05% standard deviation across the spectrum 0.35–2.5 μm. The spectroradiometer optic cable is mounted in the contact probe at a fixed view zenith angle of 35° in the same azimuth about the probe axis as the light source.

The contact probe is retrofitted with a black, slip-on circular spacer that maintains a constant 1 cm distance from the probe lens to the snow face. This spacing is necessary to prevent grain growth and snowmelt from conduction of energy from the light source through the probe. Moreover, the spacer maintains consistent illumination from spectrum to spectrum by occluding all illumination other than that from the probe. In low-density snow the user must maintain slight contact of the spacer rim with the surface. While we have not evaluated the sensitivity of retrievals to changes in orientation of the probe from surface normal, the model's insensitivity to changes in illumination (topography) should

accommodate slight changes in probe orientation. The instantaneous field of view of the field spectroradiometer through the contact probe is nominally 1.1 cm, but with the slip-on spacer the instantaneous field of view is 2.1 cm.

Vertical OGR stratigraphy was determined from contiguous measurements every 2 cm vertically. Snow layers thinner than 2 cm are averaged with the adjacent layers and are therefore not represented in our grain-size stratigraphy. Similarly, the horizontal stratigraphic variations were mapped on a rectangular grid to create an OGR map of the snow-pit face. The contact probe with spacer is first oriented normally to a Spectralon (http://www.labsphere.com) reflectance standard for initial spectral measurements of the surface illumination and then oriented normally to the vertical snow-pit surface for measurement of the reflected spectrum. The reflectance standard has a directional-hemispherical reflectance calibration spectrum, provided by the manufacturer, that lies near 0.98–0.99 across most of the spectrum (Bruegge and others, 2001). However, the hemispherical-directional reflectance (used here in conical measurements of reflected radiance) of the Spectralon panel itself varies up to 10% away from Lambertian reflectance, depending on the viewing and illumination geometry (Sandmeier and others, 1998). Given that the illumination and view geometries are fixed with the contact probe, we consistently correct for this anisotropy using the hemispherical-directional reflectance factor (HDRF) calibration spectrum for the $\theta_i = 0°$ and $\theta_v = 35°$ (R.O. Green, unpublished data) incident and viewed zenith angles, respectively. Bruegge and others (2001) demonstrated that the anisotropic reflectance of Spectralon panels is relatively invariant from panel to panel.

Snow pits are dug to the desired depth for sampling; in the San Juan Mountains, Colorado, the snow pits were dug to the ground (1–4 m), whereas in Greenland the snow pits were dug to the snow–ice interface ($\sim$2 m). For each column, we collect ten spectra of the Spectralon panel at the beginning of a column acquisition and then collect duplicate, contiguous spectra at each 2 cm layer of the snow-pit face (Fig. 2). For single-column stratigraphy, we follow the snow sampling with ten more spectra of the Spectralon panel and interpolate the white standard spectra across the acquisitions of snow to account for any instrument drift (Schaepman and Dangel, 2000). For imaging of the snow-pit face, each column is preceded by ten spectra of the Spectralon panel. The imaging grid was established with construction fencing that has regular nodes of 6 cm horizontally and vertically, to which each cell was attributed a spectrum and an OGR.

Spectroscopy model

ASD-FR spectra collected using the above protocols are inverted for OGR using the validated Nolin–Dozier (ND) model from the integral of the continuum-scaled ice absorption band centered at $\lambda \cong 1.03\,\mu m$. The ND model has a grain-size uncertainty of ±10–$50\,\mu m$ across the grain radius range of 50–900 μm (Nolin and Dozier, 2000). As the model has already been repeatedly validated in field applications for nadir views of the snow surface with stereological analyses (Davis and others, 1993; Nolin and Dozier, 2000; Painter and others, 2003; Painter and Dozier, 2004), we do not perform a redundant validation here. However, a complete sampling of all ranges of OGR and morphology has yet to be performed.

Fig. 2. Contact probe in use in the San Juan Mountains.

The model is based on the spectroscopic quantification of the absorption represented by a local absorption feature relative to the continuum spectrum and its non-linear relationship to grain size (absorbing path length). The breadth and depth of this ice absorption feature increase with increasing grain size. The model relates snow grain size to the summation $I_{1.03}$:

$$I_{1.03} = \sum_{\lambda=0.95\,\mu m}^{1.09\,\mu m} \frac{R_{c\lambda} - R_{s\lambda}}{R_{c\lambda}} \Delta\lambda, \qquad (1)$$

where $R_{c\lambda}$ is the continuum reflectance (HDRF) at wavelength λ and $R_{s\lambda}$ is the snow reflectance across the wavelength range, $\Delta\lambda$ (Fig. 3). The continuum reflectance is the reflectance interpolated between the shoulders of the absorption feature and represents the reflectance in the absence of ice absorption. Scaling by the continuum reflectance accounts for variability in irradiance that can be caused by topography or, in the case of contact spectroscopy, slight deviations of the contact probe from nadir (e.g. in the case of low-density snow).

Snow directional reflectances (HDRF) were generated for grain radii ranging from 10 to 1100 μm for the illumination and viewing geometries of the contact probe using the radiative transfer modeling described by Nolin and Dozier (2000) and Painter and Dozier (2004). This approach determines the single scattering properties for spheres using the Mie approach (Mie, 1908) and, with these, determines the HDRF from the discrete ordinates solution to the radiative transfer equation (Stamnes and others, 1988). For each HDRF spectrum varying across grain radius, Equation (1) is computed to generate the inversion look-up table.
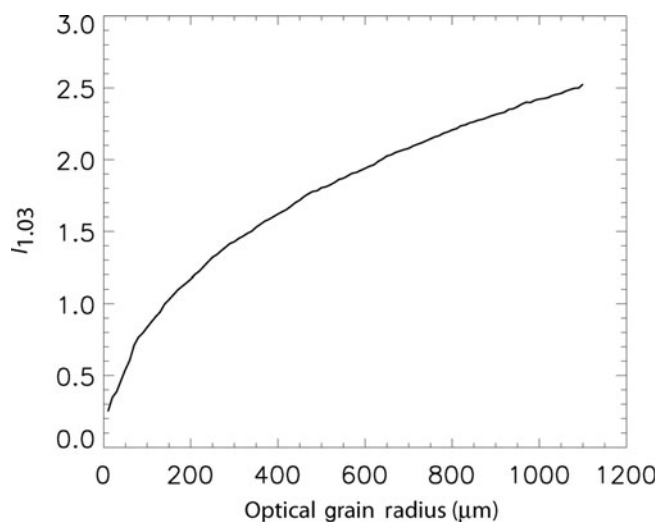
Fig. 3. Dependence of the integral of the ice absorption feature with maximum at 1.03 μm on optical grain radius, for the illumination and view geometry of the contact probe.

Fig. 4. Grain-size stratigraphy for same basin location in the Senator Beck Basin on 18 April, 18 May and 14 June 2005. Solid bars and dashed bars at left indicate ice layers and dust layers, respectively, with color coding according to date of acquisition. These data show the advance of snow metamorphism and the development of grain coarsening and layer freezing in the surface layers due to enhanced snowmelt from dust deposition.

SITES

San Juan Mountains snow pits

Snow pits were excavated at seven sites in the Senator Beck Basin, Colorado (37°55′ N, 107°43′ W) on a monthly basis in April–June 2005. The snow pits were sampled in the context of the field campaigns for the US National Science Foundation (NSF) Atmospheric Sciences project 'Radiative effects of desert dust deposits in alpine snow'. With the contact probe, we collected duplicate spectra at each 2 cm layer for the entire snow-pit depths. At the same time, TGR, density, snow temperature and snow hardness were sampled in stratigraphy. We present results from 18 April, 18 May and 14 June for an alpine, south-facing pit at 3882 m elevation, where snow depths ranged from 95 to 191 cm.

Greenland snow pits

Snow pits were excavated upwind of Swiss Camp, Greenland (69°34′06″ N, 49°18′57″ W). Pit faces were oriented perpendicular to the long axis of single sastrugi features, i.e. perpendicular to the prevailing katabatic winds. The periodicity of the short axis of the sastrugi features was approximately 2 m and thus pits were 2 m wide. Once the pit was excavated, the upwind wall was shaved smooth for analysis. Snow density measurements were taken at 10 cm vertical intervals over the entire snow-pit depth (i.e. from the snow–atmosphere interface to the snow–ice interface) using a 1 L stainless-steel cutter. Snow temperature measurements were made at 10 cm increments and at the two interfaces using a digital thermometer.

RESULTS

San Juan Mountains

Figure 4 shows OGR stratigraphy for the same snow pit in the Senator Beck Basin during the three field campaigns in spring 2005. Snow depths of the pits were 173 cm on 18 April, 192 cm on 18 May and 96 cm on 14 June. The OGR stratigraphy data shown here indicate the dramatic transformation of the grain sizes of surface layers in response to dust loading and subsequent enhanced snowmelt.
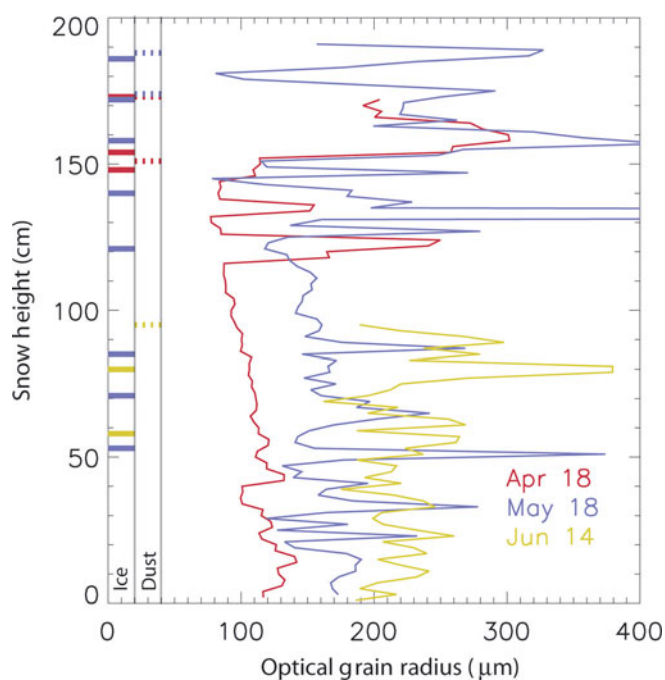
In April, the snow surface layer OGR had already coarsened in response to dust deposition on 23 March, 4 April and 8 April (Fig. 4) coupled with a period of full potential surface irradiance. Intense melt resulted in infiltration of liquid water that refroze to form ice layers at the surface and depths of 154 cm (1 mm ice) and 148 cm (0.5 mm ice), and significant OGR increase in the layers from 150 cm to the surface at 173 cm. Below the coarse layers at 115–125 cm, OGRs were significantly smaller, ranging from 80 to 120 μm, increasing with depth.

By 18 May, additional coarsening occurred in response to the fourth dust deposition (9 May) and intense melt during further clear periods. This resulted in a coarse layer and an ice layer in the top 10 cm. At depth, the same complexes of ice layers and large OGRs at depths of 150–170 and 120–135 cm occurred. Below these layers, OGRs were consistently ∼50 μm larger than in April except at distinct ice and larger grain layers from melt infiltration through flow fingers and layer pooling at textural discontinuities (Kattelmann and Dozier, 1999).

After ablation commenced between the May and June acquisitions, surface OGR increased to 250–350 μm. The high vertical frequency variability in OGR remained at depth, and the general grain size increased again by 50–100 μm. The complexes of coarse grains and ice layers remained in the 14 June stratigraphy but were displaced to ∼80 and ∼60 cm, respectively (note the ice layer placements and dust layer placements for 14 June).

Greenland

Figure 5 shows OGR images and snow density and temperature profiles for the snow pits sampled on 5 and 17 May 2005 at Swiss Camp. OGR variability decreased
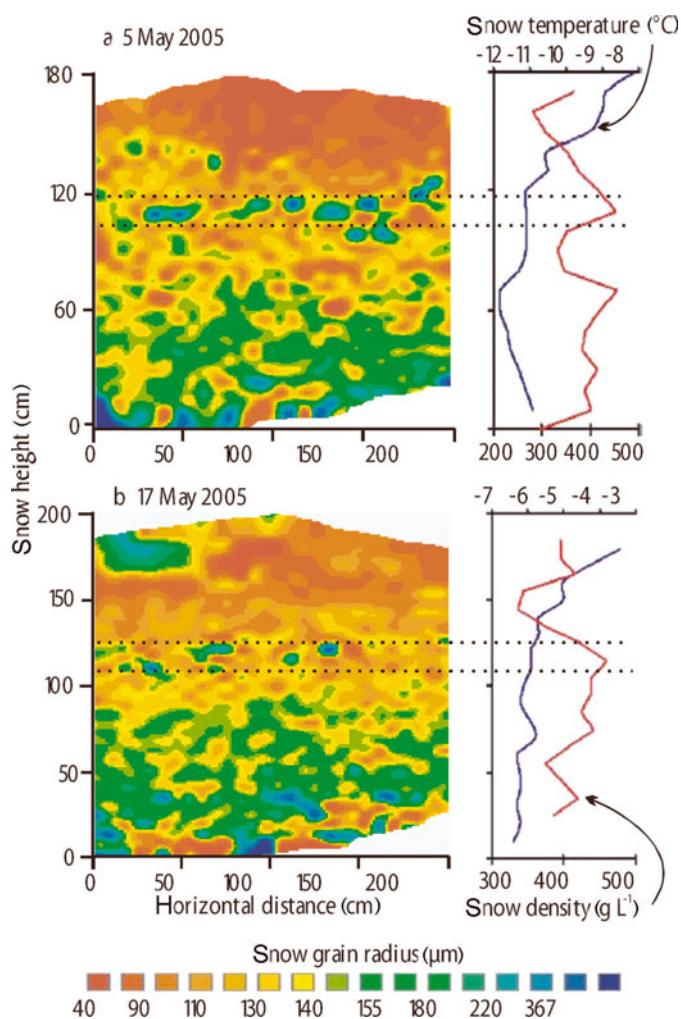
Fig. 5. OGR image for snow pit at Swiss Camp on 5 and 17 May 2005. Snow height is relative to the distinct snow–ice interface. Horizontal dotted lines show the location of a 9 cm thick melt–freeze complex.
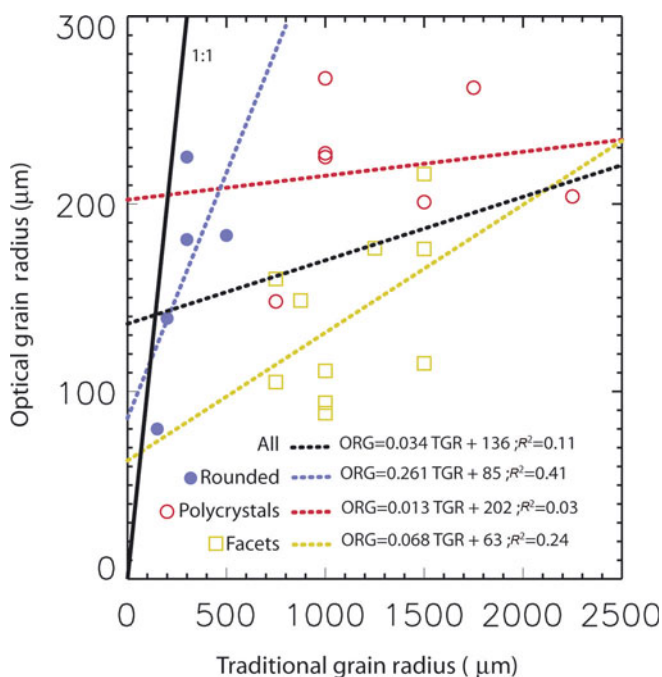

Fig. 6. OGR vs TGR for rounded grains, polycrystals and faceted forms as defined by Colbeck and others (1990). The 1:1 line is given as the solid black line. Individual linear regressions are given by dashed colored lines corresponding to the color of the grain morphology symbol, and the linear regression for all grain morphologies is given by the dashed black line.

by 18% between the two sampling periods. Slight increases (3%) in mean OGR were observed, with maximum OGR increasing by 22%. The spectral retrieval method well characterized general trends in snow OGR, with larger faceted grains at depth and smaller rounded grains near the surface. Vertically discrete features such as melt–freeze complexes were also detected (Fig. 5).

Snow temperature profiles indicated significant warming of the snowpack (average of 47%) between the two acquisition periods. Snow density variability decreased by 13% and mean snow density increased by 8%. The increased snow temperature, grain size and density, combined with the lower variability in density, suggest advancement in snowpack metamorphic state and ripening. Snow grain morphology changed little between the two acquisitions, but snow wetness increased as surface melting began, on about 15 May, resulting in saturation of surface layers to a depth of approximately 50 cm on 17 May.

DISCUSSION

Measured spectra across the ice absorption feature centered at $\lambda = 1.03\,\mu m$ are inverted with the model developed by Nolin and Dozier (2000) with apparent uncertainties of

10–50 μm. However, we suggest that the maximum uncertainty is >50 μm, based on other measurements and modeling results (Painter and others, 2003; Painter and Dozier, 2004) that indicate that the uncertainty is ∼100 μm for radii < ∼300 μm (e.g. fig. 12 of Painter and others, 2003). However, because the spectral albedo of snow becomes increasingly degenerate with increasing OGR (Fig. 3) (Wiscombe and Warren, 1980), this greater uncertainty in OGR of ∼100 μm has decreasing effects on radiative transfer calculations with increasing OGR.

We compared the grain sizes inferred as OGR and TGR at the same layers from the snow pits of the San Juan Mountains (Fig. 6). Across all grain morphologies, the relationship between OGR and TGR was proportional but with little variance ($R^2 = 0.11$) and root-mean-square error (rmse) 966 μm. For just rounded grains, the relationship was most robust with the least scatter ($R^2 = 0.41$) and roughly order-of-magnitude smaller error (160 μm rmse). For polycrystals and faceted grains, the relationships between OGR and TGR were weaker ($R^2 = 0.03$ and 0.24, respectively) and with significantly larger errors (1206 and 1010 μm rmse, respectively). These data suggest that only in the case of rounded grains would hand-lens measurements have the potential for estimating OGR; but far more sampling is required to firmly establish this result. However, this result is not unexpected, because of the relative ease of estimating radii for a collection of spherical grains as opposed to estimating effective radii for non-spherical polycrystals or facets.

To properly demonstrate the utility of contact spectroscopy OGR for radiative transfer modeling, we compared shortwave spectral albedo measurements with model results. On 16 May 2006, as part of a field campaign at Senator Beck Basin, the spectral albedo was measured with an ASD-FR
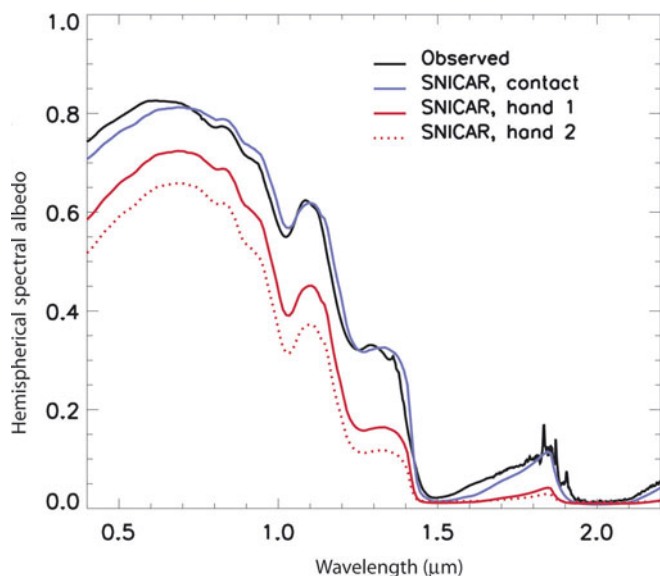
Fig. 7. Hemispherical spectral albedo measurements and the snow, ice and aerosol radiative model (SNICAR) results. Contact indicates OGR stratigraphy was inferred from contact spectroscopy; hand 1 is half of the minimum TGR, and hand 2 is half (radius) of the mean TGR.

with a cosine receptor for hemispheric spectral flux measurements. Spectral albedo, α_λ, was calculated from the ratio of reflected hemispheric flux (in digital numbers, $DN_{\lambda,reflected}$) with incident hemispheric flux ($DN_{\lambda,incident}$):

$$\alpha_\lambda = \frac{DN_{\lambda,\,reflected}}{DN_{\lambda,\,incident}}. \qquad (2)$$

We modeled spectral albedo with the snow, ice and aerosol radiative model (SNICAR) (Flanner and Zender, 2006). Snow grain-size boundary conditions for the model came from contact spectroscopy and hand-lens estimates all made on 16 May 2006. In this case, OGR from contact spectroscopy ranged from 139 to 303 μm in the top 30 cm. Two sets of stratigraphies came from hand-lens estimates: (1) half the smallest dimension determined from hand-lens estimates (range 500–1000 μm) and (2) half the mean dimension determined from hand-lens estimates (range 750–2000 μm). Snow impurity concentration was determined from gravimetric filtrations. An impurity mixture of 1% by mass Fe_2O_3 and 700 ppb black carbon was used to represent the reduction in visible albedo.

Figure 7 shows the measurements and modeling results. The SNICAR 'contact' result accurately represents the spectral albedo to 0.02 rmse in spectral albedo with direct use of the contact spectroscopy OGR stratigraphy. The SNICAR 'hand 1' and 'hand 2' results, driven by TGR described above, have significant albedo errors of 0.10 and 0.15 rmse, respectively. These albedo errors result directly from the much larger absorbing path length estimated from the subjective hand-lens approach that does not account for high spatial variability in the grain morphology and air inclusions. We determine the spectrally integrated net shortwave radiation, K^*, from the irradiance spectrum, K_λ, for the time of acquisition and the spectral albedo, α_λ:

$$K^* = \sum_{\lambda=0.305\mu m}^{2.805\mu m} (1-\alpha_\lambda)K_\lambda\,\Delta_\lambda. \qquad (3)$$

The irradiance spectrum comes from the Santa Barbara DISORT atmospheric radiative transfer (SBDART) (Ricchiazzi and others, 1998) for the same atmosphere and time as the acquisition. The errors in modeled net shortwave radiation were 8, 94 and 143 $W\,m^{-2}$, respectively, for contact, hand 1 and hand 2 stratigraphies.

CONCLUSIONS

We have introduced a contact spectroscopy technique for retrieval of the stratigraphy or spatial stratigraphy of snow OGR. The technique is a coupling of an ASD FieldSpec FR field spectroradiometer with a modified ASD contact probe with an autonomous light source. Applications in both alpine and arctic environments indicate that the technique provides a robust and rapid method for observing snowpack stratigraphy with unprecedented quantitative detail.

The observed differences between OGR and TGR, as well as the modeled albedo and net shortwave calculations associated with them, suggest that the empirical relationships of snow metamorphism and grain growth currently employed in snow models probably require a fundamental revision and re-parameterization if grain size as calculated by the model is to be validated and useful for remote sensing and shortwave radiation calculations. The term 'grain size' has been used loosely in the snow literature, largely due to poor definition of the exact physical meaning and the differences in meaning depending on the application. In the case of optical remote sensing and radiative transfer calculations, the specific surface area (surface area to volume ratio) is a more useful measure, whereas in mechanical applications the bond density, size and morphology are more useful.

More measurements across the coupled space of snow grain morphology and specific surface area are needed to absolutely determine the appropriateness of model assumptions of spheres. However, Painter and Dozier (2004) demonstrated with limited hyperspectral goniometer measurements of snow directional reflectance and radiative transfer calculations that the assumption of spheres results in less than 5% reflectance error in most of the angular domain where $\theta_v < 40°$ (such is applicable to the contact spectroscopy model). Additionally, these measurements were performed without completely covering the snow pit to eliminate all additional irradiance. The black spacer on the contact probe eliminates ambient irradiance into the contact probe's illumination field, but, as noted by Matzl and Schneebeli (2006), some ambient irradiance can be multiply scattered into the illumination and reflectance fields. This problem is, however, likely to be minor given that the in-pit sky- and terrain-reflected radiance at 1.03 μm is significantly smaller than the irradiance from the contact probe and the transmission of radiation at this wavelength in snow is sufficiently low that >97% of intensity is removed in less than 1 cm of snow depth (Beaglehole and others, 1998). Nevertheless, in future acquisitions we will evaluate the sensitivity of retrievals to complete cover of the snow pit with an opaque sheet to eliminate all sky- and terrain-reflected irradiance.

The measurements of OGR stratigraphy are currently being used in collaborations for the development of snow albedo modeling. Potential applications include modeling of radiative properties such as lidar backscattering and snow- depth retrievals, microwave emission from layered

snow cover and improved inference of snow depth and SWE, and improved validation and restructuring of snow process models.

The next logical step in development of this approach is to couple it with the high-spatial-resolution photographic technique (Matzl and Schneebeli, 2006). With snow-pit face regions well characterized in hyperspectral reflectance and OGR by the contact probe method, reflectances inferred by the photographic technique can then be mapped quantitatively to produce a high-resolution and accurate map of OGR stratigraphy.

ACKNOWLEDGEMENTS

REFERENCES

Armstrong, R.L., A. Chang, A. Rango and E. Josberger. 1993. Snow depths and grain-size relationships with relevance for passive microwave studies. *Ann. Glaciol.,* **17**, 171–176.

Bartelt, P. and M. Lehning. 2002. A physical SNOWPACK model for the Swiss avalanche warning. Part I. Numerical model. *Cold Reg. Sci. Technol.,* **35**(3), 123–145.

Beaglehole, D., B. Ramanathan and J. Rumberg. 1998. The UV to IR transmittance of Antarctic snow. *J. Geophys. Res.,* **103**(D8), 8849–8858.

Bruegge, C., N. Chrien and D. Haner. 2001. A Spectralon BRF data base for MISR calibration applications. *Remote Sens. Environ.,* **77**(3), 354–366.

Brun, E., P. David, M. Sudul and G. Brunot. 1992. A numerical model to simulate snow-cover stratigraphy for operational avalanche forecasting. *J. Glaciol.,* **38**(128), 13–22.

Colbeck, S.C. 1991. The layered character of snow covers. *Rev. Geophys.,* **29**(1), 81–96.

Colbeck, S.C. *and 7 others.* 1990. *The international classification for seasonal snow on the ground.* Wallingford, Oxon., International Association of Hydrological Sciences. International Commission on Snow and Ice.

Davis, R.E., J. Dozier and R. Perla. 1987. Measurement of snow grain properties. *In* Jones, H.G. and W.J. Orville-Thomas, *eds. Seasonal snowcovers: physics, chemistry, hydrology.* Dordrecht, etc., D. Reidel Publishing Co., 63–74. (NATO ASI Series C: Mathematical and Physical Sciences 211.)

Davis, R.E., A.W. Nolin, R. Jordan and J. Dozier. 1993. Towards predicting temporal changes of the spectral signature of snow in visible and near-infrared wavelengths. *Ann. Glaciol.,* **17**, 143–148.

Dozier, J. 1989. Spectral signature of alpine snow cover from the Landsat Thematic Mapper. *Remote Sens. Environ.,* **28**, 9–22.

Durand, M. and S.A. Margulis. 2006. Feasibility test of multi-frequency radiometric data assimilation to estimate snow water equivalent. *J. Hydromet.,* **7**(3), 443–457.

Flanner, M.G. and C.S. Zender. 2006. Linking snowpack microphysics and albedo evolution. *J. Geophys. Res.,* **111**(D12), D12208. (10.1029/2005JD006834.)

Foster, J.L. *and 6 others.* 2005. Quantifying the uncertainty in passive microwave snow water equivalent observations. *Remote Sens. Environ.,* **94**(2), 187–203.

Grenfell, T.C. and S.G. Warren. 1999. Representation of a nonspherical ice particle by a collection of independent spheres for scattering and absorption of radiation. *J. Geophys. Res.,* **104**(D24), 31,697–31,709.

Jin, J. *and 7 others.* 1999. One-dimensional snow water and energy-balance model for vegetated surfaces. *Hydrol. Processes.,* **13**(14–15), 2467–2482.

Jordan, R. 1991. A one-dimensional temperature model for a snow cover: technical documentation for SNTHERM.89. *CRREL Spec. Rep.,* 91-16.

Kattelmann, R. and J. Dozier. 1999. Observations of snowpack ripening in the Sierra Nevada. *J. Glaciol.,* **45**(151), 409–416.

Kelly, R.E., A.T. Chang, L. Tsang and J.L. Foster. 2003. A prototype AMSR-E global snow area and snow depth algorithm. *IEEE Trans. Geosci. Remote Sens.,* **41**(2), 230–242.

Li, W., K. Stamnes, B. Chen and X. Xiong. 2001. Snow grain size retrieved from near-infrared radiances at multiple wavelengths. *Geophys. Res. Lett.,* **28**(9), 1699–1702.

Matzl, M. and M. Schneebeli. 2006. Measuring specific surface area of snow by near infrared photography. *J. Glaciol.,* **52**(179), 558–564.

Mie, G. 1908. Beiträge zur Optik trüber Medien, speziell kolloidaler Metallösungen. *Ann. Phys. [Berlin],* **330**(3), 377–445.

Nolin, A.W. and J. Dozier. 2000. A hyperspectral method for remotely sensing the grain size of snow. *Remote Sens. Environ.,* **74**(2), 207–216.

Painter, T.H. and J. Dozier. 2004. Measurements of the hemispherical-directional reflectance of snow at fine spectral and angular resolution. *J. Geophys. Res.,* **109**(D18), D18115. (10.1029/2003JD004458.)

Painter, T.H., J. Dozier, D.A. Roberts, R.E. Davis and R.O. Green. 2003. Retrieval of subpixel snow-covered area and grain size from imaging spectrometer data. *Remote Sens. Environ.,* **85**(1), 64–77.

Pielmeier, C. and M. Schneebeli. 2003. Developments in the stratigraphy of snow. *Surv. Geophys.,* **24**(5–6), 389–416.

Ricchiazzi, P., S. Yang, C. Gautier and D. Sowle. 1998. SBDART: a research and teaching software tool for plane-parallel radiative transfer in the Earth's atmosphere. *Bull. Am. Meteorol. Soc.,* **79**(10), 2101–2114.

Sandmeier, S., C. Müller, B. Hosgood and G. Andreoli. 1998. Sensitivity analysis and quality assessment of laboratory BRDF data. *Remote Sens. Environ.,* **64**(2), 176–191.

Schaepman, M.E. and S. Dangel. 2000. Solid laboratory calibration of a nonimaging spectroradiometer. *Appl. Opt.,* **39**(21), 3754–3764.

Stamnes, K., S.C. Tsay, W. Wiscombe and K. Jayaweera. 1988. Numerically stable algorithm for discrete-ordinate-method radiative transfer in multiple scattering and emitting layered media. *Appl. Opt.,* **27**(12), 2502–2509.

Warren, S.G. 1982. Optical properties of snow. *Rev. Geophys. Space Phys.,* **20**(1), 67–89.

Wiscombe, W.J. and S.G. Warren. 1980. A model for the spectral albedo of snow. I. Pure snow. *J. Atmos. Sci.,* **37**(12), 2712–2733.